Supplement of Clim. Past, 12, 849–869, 2016
http://www.clim-past.net/12/849/2016/
doi:10.5194/cp-12-849-2016-supplement

Climate of the Past
Open Access
EGU

Supplement of

Sea surface temperature variability in the central-western Mediterranean Sea during the last 2700 years: a multi-proxy and multi-record approach

M. Cisneros et al.

Correspondence to: Mercè Cisneros (mbermejo@ub.edu)

Supplement Information to Cisneros et al., 2016.

1 Age model development

1.1 ^{14}C, ^{210}Pb, ^{137}Cs dates

Absolute dating with radiocarbon dates was focused on cores MIN1, MIN2 and MR3.3 (Table S1). According to those dates and assuming the sampling year as the core top age (2006 and 2009, respectively), the sedimentation rates of these three cores result in 13 ± 1, 20 ± 3 and 13 ± 5 cm ky^{-1}, respectively (sedimentation rates uncertainties are expressed as 1 σ in this section).

In order to evaluate the preservation of the core tops, ^{210}Pb activity profiles were obtained from cores MIN1, MIN2, MR3.1A and MR3.2 (Fig. S1). ^{210}Pb concentrations generally decrease with depth in all four cores, down to 3.5 cm in core MIN2 and 3 cm for cores MIN1, MR3.1A and MR3.2. Excess ^{210}Pb concentrations at the surface and inventories in the cores MIN are in agreement with those published for the Algero-Balear Basin (Garcia-Orellana et al., 2009). However, they were lower in MR3 cores, particularly for core MR3.1A, which we attribute to the loss of the most surficial part of these cores during recovery, corresponding to about 50 yr by comparison to the other cores. The variability in the ^{210}Pb data denotes the high heterogeneity of this sedimentary system in reference to deep-sea hemipelagic sediments, highlighting the relevance of its study on the basis of a multicore approach (e.g. Maldonado et al., 1985; Martin et al., 1989; Calafat et al., 1996; Velasco et al., 1996; Canals et al., 2006; Frigola et al., 2007).

The concentration profile and inventory of ^{137}Cs in core MIN1 is also in good agreement with the results reported for the western Mediterranean Basin (Garcia-Orellana et al., 2009). Its detection down to 3 cm combined with the excess ^{210}Pb

concentration profile suggests the presence of sediment mixing to be accounted for in the calculation of the sediment accumulation rates, which are to be taken as maxima estimates. In doing so, the maxima sedimentation rates for the last 100–150 years are: 27 ± 2 cm kyr^{-1} (core MIN1), 28 ± 2 cm kyr^{-1} (MIN2), 28 ± 4 cm kyr^{-1} (MR3.1A), and 35 ± 3 cm kyr^{-1} (MR3.2). These sedimentation rates are in agreement with those previously described in a long sediment record recovered within the contouritic system (Frigola et al., 2007 and 2008), but much higher than those found in the literature from deeper sites of the Balearic Sea, with predominant hemipelagic sedimentation (e.g. Weldeab et al., 2003; Zúñiga et al., 2007; Garcia-Orellana et al., 2009).

1.2 Biostratigraphical data based on planktonic foraminifera

Core MR3.3, the best ^{14}C-dates time-constrained, was chosen in order to perform a taxonomic analysis of planktonic foraminifera. The identified species were: (1) *Globigerina bulloides* including *G. falconensis*, (2) *Globigerinoides ruber* pink and white variety, (3) *Orbulina* spp. including both *O. universa* and *O. suturalis*, (4) *Globigerinoides quadrilobatus* and *G. sacculifer*, (5) *Globigerinatella siphoniphera* including *G. calida*, (6) *Globorotalia inflata*, (7) *Turborotalita quinqueloba*, (8) *Globigerinita glutinata*, (9) *Neogloboquadrina pachyderma* right coiled, (10) *Neogloboquadrina dutertrei*, (11) *Globorotalia truncatulinoides* left coiled and (12) *Clavoratorella* spp. The abundance of *G. truncatulinoides* left coiled was also analysed in the top of the core MR3.1A.

In order to improve the time constrain of our cores, percentages records of *G. quadrilobatus* and *G. truncatulinoides* left coiled from core MR3.3 have been correlated with those from a southern Tyrrhenian Sea composite core (Fig. S2), with a very robust age-model (Lirer et al., 2013) based on the combination of different dating methods (radionuclides-^{14}C AMS dates and tephra-chronology). The Mediterranean eco-

biostratigraphic strength of of these taxa has been previously documented by Piva et al. (2008) for the last 370ky. The pronounced decrease in *G. quadrilobatus* percentages at the base of core MR3.3 (Fig. S2a) can be correlated with the end of the *G. quadrilobatus* acme interval observed in the north and south Tyrrhenian Sea record (Lirer et al., 2013, 2014; Di Bella et al., 2014) from 1750 to 750 BCE and previously documented in the Sicily Channel (Sprovieri et al., 2003) and the Sardinian valley (Budillon et al., 2009). In addition, data on distribution pattern of the leaving planktonic foraminifera, reported in Pujol and Vergnaud-Grazzini (1995), documented that this taxon is present in the whole central and south western Mediterranean (excluding the GoL). This correlation provide to us a control age point in core MR3.3 of 750 ± 48 BCE at about 27 cm, consistent with the ^{14}C dating of 301 ± 87 BCE at 24 cm. In the upper part of the MR3.3 record, another control age point can be obtained from the correlation of the pronounced peak of *G. truncatulinoides* left coiled (~20% in abundance, Fig. S2b) with a similar peak previously reported in the central and south Tyrrhenian Sea record during the LIA at 1718 ± 10 CE (Lirer et al., 2013; Margaritelli et al., 2015), and coincident with the Maunder event (Vallefuoco et al., 2012; Lirer et al., 2014; Margaritelli et al., 2015). Thunell (1978) documented the occurrence in recent surface sediments of this taxon from Balearic Islands to Sicily channel and Pujol and Vergnaud-Grazzini (1995) observed this species in leaving abundance foraminifera of the whole western Mediterranean. This age point is also consistent with the obtained ^{14}C date of core MR3.3 at 3.5cm of 1434 ± 51 CE, further supporting the absence of the last two centuries in the core MR3.3. The absence of these centuries is also suggested by the *G. truncatulinoides* left coiled abundance patterns data from the top (1.5–3.5 cm) of the core MR3.1A (Fig. S2b). MR3.1A data is in agreement with the drop of the peak in core MR3.3 and ^{210}Pb measurements (Fig. S1) have corroborated the presence of the most recent sediment in core MR3.1A.

1.3 Bayesian accumulation models

A preliminary age model for cores MIN1, MIN2 and MR3.3 was initially generated by means of available ^{14}C ages, the two biostratigraphical dates from core MR3.3 and maximum sedimentation rates derived from ^{210}Pb concentration profiles from cores MIN1 and MIN2. This preliminary age model was built using the Bayesian statistics software Bacon with the statistical package R (Blaauw and Christen, 2011).

Considering that the two independent sedimentation rates estimations based on ^{14}C and ^{210}Pb have significant uncertainties inherent to the methods and considering the different sampling resolution, averaged sedimentation rates obtained from the two methods have been taken into account in the Bayesian accumulation models. Regarding the core top ages, it was considered to be the recovering year (2006 ± 10 CE) in MIN cores and 1718 ± 10 CE for core MR3.3, coinciding with the peak in the *G. truncatulinoides* record. The program settings for thickness of the sections and memory were chosen to fulfil the criterions of the best mean 95% confidence range and to maintain good correlation between prior and posterior accumulation rates. In addition, it was decided to keep the memory strength values rather high since the sedimentary context, a contouritic drift, is expected to record highly variable accumulation rates, and due to the smother changes induced by lowering the memory strength would no reflect realistic changes in this context.

The best Bayesian models achieved with a confidence mean of 95% provide accumulation rates for cores MIN1, MIN2 and MR3.3 of 14 ± 2, 22 ± 1 and 12 ± 1 cm kyr^{-1}, respectively (uncertainties are expressed as 1 σ), which correspond to mean time resolutions of 292, 161, and 200 yr, respectively. It should be noted that the largest errors are obtained for core MIN1 because of the only two ^{14}C dates. These age models reconstruct a rather smooth accumulation history, although significant fluctuations in accumulation rate at centennial or even decadal scale can be expected in this

sedimentological context. The posterior outputs for accumulation rate (see Fig. S3) and its variability are quite comparable to their prior ones, but in the case of core MR3.3 the posterior output indicates larger memory (more variability) than that assumed a priori. This is due to the strong change in sedimentation rates at about 12 cm (998 CE) that the prior output tends to attenuate, and which could be associated with abrupt changes in sedimentation rates at that time (Fig. S3c).

These age models have been then further re-evaluated using other geochemical proxies as stratigraphical tools in order to ensure a common chronological framework for the obtained climate records (Sect. 1.4 Suppl. Info.). Nevertheless, any readjustment has always been kept within the confident rage of the Bayesian models.

1.4 Multi-proxy chronostratigraphy

The chronologies of cores MIN1, MIN2 and MR3.3 were finally evaluated and readjusted in base to their Mg/Ca records and taking into account the 95% probability intervals obtained in the Bayesian models.

Mg/Ca measured in *G. bulloides* is a well-established proxy of Sea Surface Temperatures (Barker et al., 2005). The two sampling stations are only separated by 30 km and thus it is a reasonable assumption to expect comparable and synchronous SST changes in all the studied cores. Visual comparison of the MIN1, MIN2 and MR3.3 records of Mg/Ca show several resemblances in some of the main patterns and structures, which are considerably synchronous with the Bayesian age models (Fig. S4). Consequently, the three records have been tuned in base to the main structures and taking into account the 95% confidence of the statistical produced models (Fig. S4). The final age-models of cores MIN1, MIN2 and MR3.3 have an average age difference that is below 24 years in reference to the Bayesian models and the 75–63% of the records are into the confidence intervals obtained in the Bayesian models.

The chronology from core MR3.3 has been the base to construct the age model

for the other MR3 cores (MR3.1A, MR3.1B and MR3.2) for which no ^{14}C dates were available (Table S2). The chronostratigraphical tools for core MR3.1 have been again the Mg/Ca records (Fig. S4; Table S4). Additionally, manganese records in all MR3 cores have also been used as an additional chronostratigraphical tool. Mn presence in deep-sea sediments is related to redox processes (Calvert and Pedersen, 1996). Considering that all MR3 cores correspond to the same multicore these Mn rich layers have been used as isochrones. The available Mn records have been measured by two different methods: Mn measured in the bulk sediment by means of XRF Core-Scanner (MR3.1B and MR3.2) and Mn present in the foraminiferal samples and measured by ICP-MS (MR3.3, MR3.1A and MR3.1B). Absolute values were very different between those samples measured with ICP-MS after cleaning the foraminifera with the reductive step (MR3.1A) and those without this cleaning step (MR3.3 and MR3.1B) but the same main features can be correlated between the three cores (Fig. S5; Table S4). In the case of core MR3.1B (Fig. S5b), analysed at ultra-high resolution (0.25 cm slides), the Mn record shows the highest values with peaks over 80 ppb whose Mg/Ca values have been excluded of derived SST records since Mn enrichments can bias Mg/Ca ratios toward higher values and lead to significant overestimation of past seawater temperatures (Boyle, 1983; Pena et al., 2005, 2008). The top 5 cm of cores MR3.1A and MR3.2 have been dated according to the maxima sedimentation rates using the ^{210}Pb flux.

1.5 Final age models and associated sedimentation rates

According to the obtained chronologies, the period covered by the studied sedimentary sequences is from 759 ± 20 BCE to 1988 ± 18 CE (uncertainties are expressed as the time resolution of the respective core here and in 1σ on the rest of this section), being core MR3.1B the one spanning a longer period (Table S3). Total average of mean accumulation rates is 17 ± 4 cm ky^{-1} with a total mean resolution of 84 ± 18 years.

The final mean sedimentation rates obtained in MIN cores, 14 ± 6 and 25 ± 10 cm kyr^{-1}, are very similar with those derivated from Bayesian model simulations, 14 ± 2 and 22 ± 1 cm kyr^{-1}, and those previously published by Moreno et al. (2012), 19 and 23 cm kyr^{-1}. The differences in sedimentation rates between all cores except MIN2 are lower than 3 cm kyr^{-1}, variability that is reasonable due the diverse sediment processes that affect the contouritic system.

References

Barker, S., Cacho, I., Benway, H., and Tachikawa, K.: Planktonic foraminiferal Mg/Ca as a proxy for past oceanic temperatures: a methodological overview and data compilation for the Last Glacial Maximum, Quaternary Sci. Rev., 24, 821–834, doi:10.1016/j.quascirev.2004.07.016, 2005.

Blaauw, M. and Christen, J. A.: Flexible paleoclimate age-depth models using an autoregressive gamma process, Bayesian Anal., 6, 457–474, doi:10.1214/11-BA618, 2011.

Boyle, E. A.: Manganese carbonate overgrowths on foraminifera tests, Geochim. Cosmochim. Ac., 47, 1815–1819, 1983.

Budillon, F., Lirer, F., Iorio, M., Macri, P., Sagnotti, L., Vallefuoco, M., Ferraro, L., Innangi, S., Sahabi, M., and Tonielli, R.: Integrated stratigraphic reconstruction for the last 80 kyr in a deep sector of the Sardinia Channel (Western Mediterranean), Deep-Sea Res Pt. II, 56, 725–737, 2009.

Calafat, A. M., Casamor, J., Canals, M., and Nyeler, F.: Distribución y composición elemental de la materia particulada en suspensión en el Mar Catalano-Balear, Geogaceta, 20, 370–373, 1996.

Calvert, S. and Pedersen, T.: Sedimentary geochemistry of manganese: implications for the environment of formation of manganiferous black shales, Econ. Geol., 91, 36–47, 1996.

Canals, M., Puig, P., Madron, X. D. De, Heussner, S., Palanques, A., and Fabres, J.: Flushing submarine canyons, Nature, 444, 354–357, doi:10.1038/nature05271, 2006.

Di Bella, L., Frezza, V, Bergamin, L., Carboni, M. G., Falese, F., Mortorelli, E., Tarragoni, C., and Chiocci, F. L.: Foraminiferal record and high-resolution seismic stratigraphy of the Late Holocene succession of the submerged Ombrone River delta (Northern Tyrrhenian Sea, Italy), Quatern. Int., 328–329, 287–300, 2014.

Frigola, J., Moreno, A., Cacho, I., Canals, M., Sierro, F. J., Flores, J. A., Grimalt, J. O., Hodell, D. A., and Curtis, J. H.: Holocene climate variability in the western Mediterranean region from a deepwater sediment record, Paleoceanography, 22, PA2209, doi:10.1029/2006PA001307, 2007.

Frigola, J., Moreno, A., Cacho, I., Canals, M., Sierro, F. J., Flores, J. A., and Grimalt, J. O.: Evidence of abrupt changes in Western Mediterranean Deep Water circulation during the last 50 kyr: a high-resolution marine record from the Balearic Sea, Quatern. Int., 181, 88–104, doi:10.1016/j.quaint.2007.06.016, 2008.

Garcia-Orellana, J., Pates, J. M., Masqué, P., Bruach, J. M., and Sanchez-Cabeza, J. A.: Distribution of artificial radionuclides in deep sediments of the Mediterranean Sea, Sci. Total Environ., 407, 887–898, doi:10.1016/j.scitotenv.2008.09.018, 2009.

Lirer, F., Sprovieri, M., Ferraro, L., Vallefuoco, M., Capotondi, L., Cascella, A., Petrosino, P., Insinga, D. D., Pelosi, N., Tamburrino, S., and Lubritto, C.: Integrated stratigraphy for the Late Quaternary in the eastern Tyrrhenian Sea, Quatern. Int., 292, 71–85, doi:10.1016/j.quaint.2012.08.2055, 2013.

Lirer, F., Sprovieri, M., Vallefuoco, M., Ferraro, L., Pelosi, N., Giordano, L., and Capotondi, L.: Planktonic foraminifera as bio-indicators for monitoring the climatic changes that have occurred over the past 2000 years in the southeastern Tyrrhenian Sea, Integr. Zool., 9, 542–54, doi:10.1111/1749-4877.12083, 2014.

Maldonado, A., Got, H., Monaco, A., O'Connell, S., and Mirabile, L.: Valencia Fan (northwestern Mediterranean): distal deposition fan variant, Mar. Geol., 62, 295–319, 1985.

Margaritelli, G., Lirer, F., Vallefuoco, M., Bonomo, S., Cascella, A., Capotondi, L., Ferraro, L., Insinga, D. D., Petrosino, P., and Rettori, R.: Climatic variability during

the last two millennia in the Tyrrhenian Sea: evidences from planktonic foraminifera and geochemical data, XV Edizione delle "Giornate di Paleontologia" PALEODAYS2015, Palermo 17–29 Maggio 2015, 72–73, Società Paleontologica Italiana, 2015.

Martin, J., Elbaz-Poulichet, F., Guieu, C., Loce-Pilot, M., and Han, G.: River versus atmospheric input of material to the Mediterranean Sea: an Overview, Mar. Chem., 28, 159–182, 1989.

Moreno, A., Pérez, A., Frigola, J., Nieto-Moreno, V., Rodrigo-Gámiz, M., Martrat, B., González-Sampériz, P., Morellón, M., Martín-Puertas, C., Pablo, J., Belmonte, Á., Sancho, C., Cacho, I., Herrera, G., Canals, M., Grimalt, J. O., Jiménez-Espejo, F., Martínez-Ruiz, F., Vegas-Vilarrúbia, T., and Valero-Garcés, B. L.: The Medieval Climate Anomaly in the Iberian Peninsula reconstructed from marine and lake records, Quaternary Sci. Rev., 43, 16–32, doi:10.1016/j.quascirev.2012.04.007, 2012.

Pena, L. D., Calvo, E., Cacho, I., Eggins, S., and Pelejero, C.: Identification and removal of Mn-Mg-rich contaminant phases on foraminiferal tests: implications for Mg/Ca past temperature reconstructions, Geochem. Geophy. Geosy., 6, Q09P02, doi:10.1029/2005GC000930, 2005.

Pena, L. D., Cacho, I., Calvo, E., Pelejero, C., Eggins, S., and Sadekov, A.: Characterization of contaminant phases in foraminifera carbonates by electron microprobe mapping, Geochem. Geophy. Geosy., 9, Q07102, doi:10.1029/2008GC002018, 2008.

Piva, A., Asioli, A., Trincardi, F., Schneider, R. R., and Vigliotti, L.: Late-Holocene climate variability in the Adriatic Sea (Central Mediterranean), The Holocene, 18, 153–167, 2008.

Pujol, C. and Vergnaud-Grazzini, C.: Distribution patterns of live planktic foraminifers as related to regional hydrography and productive systems of the Mediterranean Sea, Mar. Micropaleontol., 25, 187–217, 1995.

Sprovieri, R., Di Stefano, E., Incarbona, A., and Gargano, M. E.: A high-resolution record of the last deglaciation in the Sicily Channel based on foraminifera and calcareous nannofossil quantitative distribution, Palaeogeogr. Palaeocl., 202, 119–142, doi:10.1016/S0031-0182(03)00632-1, 2003.

Thunell, R. C.: Distribution of Recent Planktonic Foraminifera in Surface Sediments of the Mediterranean Sea, Mar. Micropaleontol., 3, 147–173, 1978.

Vallefuoco, M., Lirer, F., Ferraro, L., Pelosi, N., Capotondi, L., Sprovieri, M., and Incarbona, A.: Climatic variability and anthropogenic signatures in the Gulf of Salerno (southern-eastern Tyrrhenian Sea) during the last half millennium, Rend Lincei, 23, 13–23, doi:10.1007/s12210-011-0154-0, 2012.

Velasco, J. P. B., Baraza, J., and Canals, M.: La depresión periférica y el lomo contourítico de Menorca: evidencias de la actividad de corrientes de fondo al N del Talud Balear, Geogaceta, 20, 359–362, 1996.

Weldeab, S., Siebel, W., Wehausen, R., Emeis, K., Schmiedl, G., and Hemleben, C.: Late Pleistocene sedimentation in the western Mediterranean Sea: implications for productivity changes and climatic conditions in the catchment areas, Palaeogeogr. Palaeocl., 190, 121–137, 2003.

Zúñiga, D., García-Orellana, J., Calafat, A., Price, N. B., Adatte, T., Sanchez-Vidal, A., Canals, M., Sanchez-Cabeza, J. A., Masqué, P., and Fabres, J.: Late Holocene fine-grained sediments of the Balearic Abyssal Plain, Western Mediterranean Sea, Mar. Geol., 237, 25–36, 2007.

Table S1. Radiocarbon dates obtained on monospecific foraminifer *G. inflata* and calibrated ages, these last one are expressed in years Before Common Era (BCE) and Common Era (CE). MR3.3 dates are presented for the first time in this study. Cores were analysed at the NOSAMS/Woods Hole Oceanographic Institution, USA (OS) and at Direct AMS Radiocarbon Dating Service, USA (D-AMS).

Laboratory Code	Core	Comp. Depth (cm)	^{14}C ages	Cal years BCE/CE (2-σ)
OS-67294	MIN1	7-7.5	895 ± 35	1411 - 1529 CE
OS-67296		19-19.5	2010 ± 35	304 - 544 CE
OS-67291	MIN2	11-11.5	845 ± 35	1440 - 1598 CE
OS-67297		18-18.5	1190 ± 35	1170 - 1312 CE
OS-67324		25-25.5	1540 ± 25	804 - 989 CE
OS-67323		28.5-29	1840 ± 30	520 - 680 CE
D-AMS 004812	MR3.3	3.5-4	938 ± 25	1383 - 1484 CE
OS-87613		6.5-7	1270 ± 35	1063 - 1256 CE
OS-87614		12-12.5	1420 ± 30	911 - 1085 CE
OS-87615		16-17	1900 ± 30	438 - 621 CE
D-AMS 004811		20-21	2350 ± 29	88 BCE - 107 CE
OS-87619		24-25	2620 ± 25	388 BCE - 214 BCE

Table S2. Summary of records analysed and methods utilized in age models.

Core	Records analysed	Age model
MIN1	Mg/Ca-SST, $U^{k'}_{37}$-SST, $\delta^{18}O$	^{14}C, ^{210}Pb, ^{137}Cs, software-simulations, SST-tuning
MIN2	Mg/Ca-SST, $U^{k'}_{37}$-SST, $\delta^{18}O$	^{14}C, ^{210}Pb, software-simulations, SST-tuning
MR3.1A	Mg/Ca-SST, $\delta^{18}O$	^{210}Pb, SST-tuning, geochemical chronostratigraphy, foraminiferal assemblage
MR3.1B	Mg/Ca-SST, $\delta^{18}O$, Geochemical composition	SST-tuning, geochemical chronostratigraphy
MR3.2	Geochemical composition	^{210}Pb, geochemical chronostratigraphy
MR3.3	Mg/Ca-SST, $U^{k'}_{37}$-SST, $\delta^{18}O$	^{14}C, software-simulations, SST-tuning, foraminiferal assemblage

Table S3. Mean accumulation rates, years covered and mean time resolution of all cores according to final age-depth models.

Core	Mean acc. rate (cm kyr^{-1})	Spanning time (yr)	Mean time resolution (yr cm^{1})
MIN1	14	2528	83
MIN2	25	1538	48
MR3.3	17	2443	78
MR3.1A	15	2635	95
MR3.1B	16	2706	98
MR3.2	15	1797	102

Table S4: Tie points used on each core to make age models with their attendant errors and indicated in Figures S4 and S5. Uncertainties correspond to the resolution of each age model on its respective core. Also absolute dates (^{14}C and biostratigraphy based on planktonic foraminiferal assemblage) are indicated. Years are expressed as before common era (BCE) and common era (CE).

Core	Composite depth (cm)	Method	Ages (years BCE/CE)	Age-uncertainties interval (years BCE/CE)
MIN1	2-2.5	Mg/Ca	1895 CE	1864-1923 CE
	6.5-7		1564 CE	1523-1606 CE
	7-7.5	^{14}C	1523 CE	1408-1523 CE
	8-8.5		1455 CE	1423-1491 CE
	10.5-11	Mg/Ca	1237 CE	1202-1315 CE
	13.5-14		1012 CE	990-1043 CE
	19-19.2	^{14}C	392 CE	295-535 CE
	20-21	Mg/Ca	234 CE	1970-289 CE
	24-24.5		63 BCE	76-11 BCE
MIN2	1-1.5		1915 CE	1887-1944 CE
	7-7.5	Mg/Ca	1580 CE	1556-1605 CE
	9-9.5		1497 CE	1485-1511 CE
	11-11.5	^{14}C	1448 CE	1440-1598 CE
	16-16.5	Mg/Ca	1263 CE	1235-1306 CE
	18-18.5		1170 CE	1170-1312 CE
	25-25.5	^{14}C	829 CE	804-989 CE
	28.5-29		651 CE	520-680 CE
MR3.3	0.5-1	Foraminiferal Assemblage	1708 CE	1708-1728 CE
	3.5-4		1484 CE	1383-1484 CE
	6.5-7		1256 CE	1063-1256 CE
	12-12.5	^{14}C	989 CE	9111085 CE
	16-17		497 CE	438-621 CE
	20-21		50 CE	88 BCE-107 CE
	24-25		388 BCE	388-214 BCE
	26-27	Foraminiferal Assemblage	702 BCE	798-702 BCE
MR3.1A	5-5.5		1627 CE	1545-1665 CE
	6.5-7	Mg/Ca	1400 CE	1350-1484 CE
	10-10.5		1050 CE	1021-1165 CE
	12.5-13		766 CE	597-824 CE
	13-13.5	Mn ICP-MS	597 CE	497-766 CE
	13.5-14	Mg/Ca	497 CE	433-597 CE
	15-16	Mn ICP-MS	254 CE	184-390 CE
	21-22	Mg/Ca	133 BCE	170 BCE-25 CE
	22-23	Mn ICP-MS	170 BCE	207 -133 BCE
	24-25		551 BCE	625-207 BCE
	26-27	Mg/Ca	702 BCE	779-625 BCE
MR3.1B	13-14	Mn-XRF	618 CE	532-702 CE
	14-14.25	Mn ICP-MS	597 CE	501-683 CE
	15-16	Mn-XRF	317 CE	65-557 CE
	16-16.25	Mn ICP-MS	254 CE	184-506 CE
	23.5-23.75		189 BCE	226-152 BCE
MR3.2	13-14	Mn-XRF	766 CE	468-824 CE
	15-16		317 CE	202-468 CE

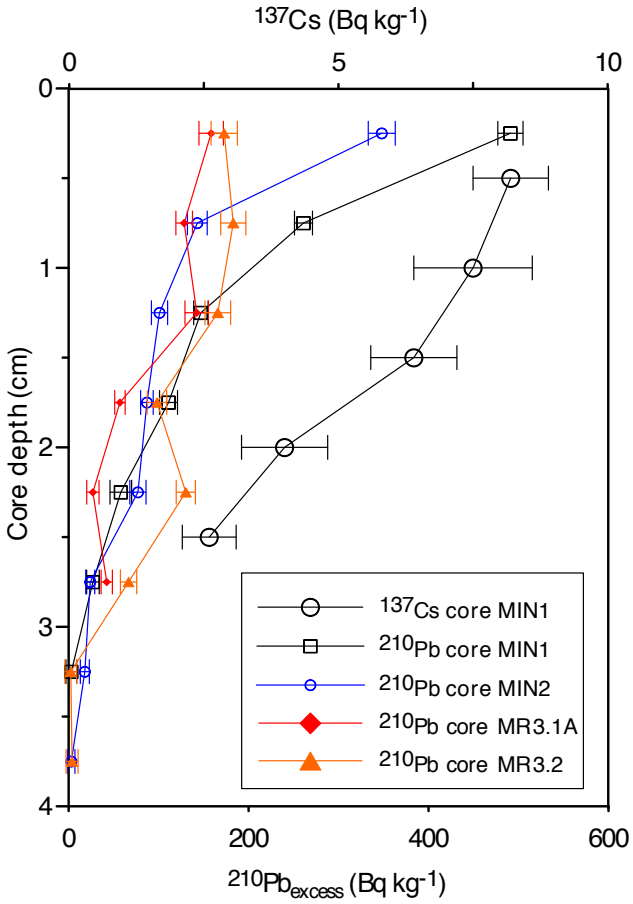

Figure S1. Excess ^{210}Pb (Bq kg^{-1}) profiles for cores MIN1, MIN2, MR3.1A and MR3.2 and also ^{137}Cs concentration profile for core MIN1. Error bars represent 1 σ uncertainty.

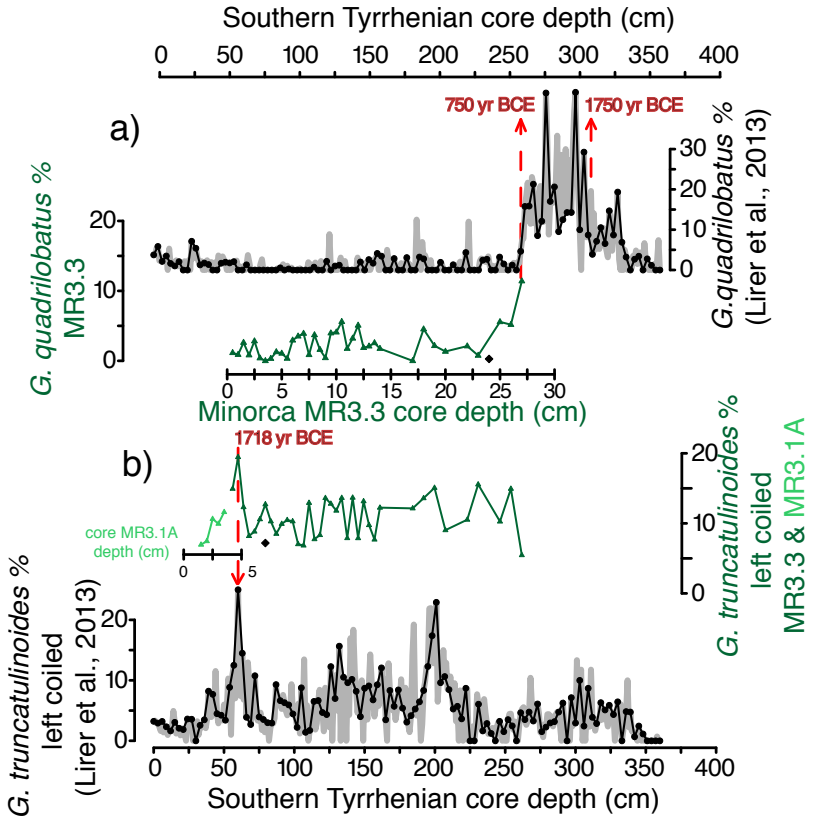

Figure S2. Comparison among the quantitative distribution patterns of (a) *G. quadrilobatus* and (b) *G. truncatulinoides* left coiled with core MR3.3 (dark green plot) and data from the composite core (C90-1m, C90 and C836 cores) studied in the southern Tyrrhenian Sea (Lirer et al., 2013), expressed as 3 point average and with the grey area corresponding to the entire record. The two tie points used in age models (dashed red line) correspond to 1718 CE and 750 BCE. Black diamonds show ^{14}C dates from core MR3.3.

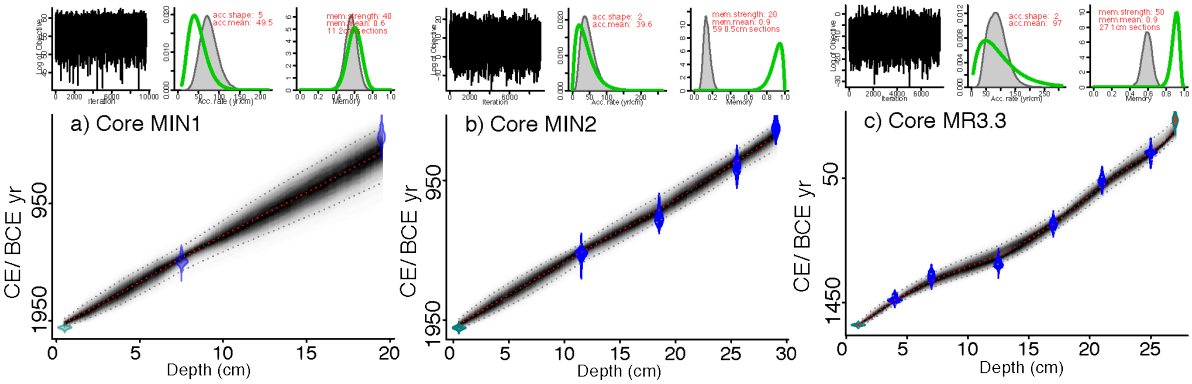

Figure S3. Age-depth models based on Bayesian accumulation simulations (Blaauw and Christen, 2011): (a) core MIN, (b) MIN2 and (c) MR3.3. The three upper plots in each core show the stable MCMC run achieved (left), the prior (green line) and posterior (grey) distributions of the accumulation rates (middle), and the prior (green line) and posterior (grey) distributions of the memory (right). Each main graphic represents the age–depth model for each core (darker grey indicates more probable calendar ages) based on the prior information, the calibrated radiocarbon dates (purple symbols), sample year for cores MIN (blue symbols) and biostratigraphical dates from core MR3.3 (red symbols).

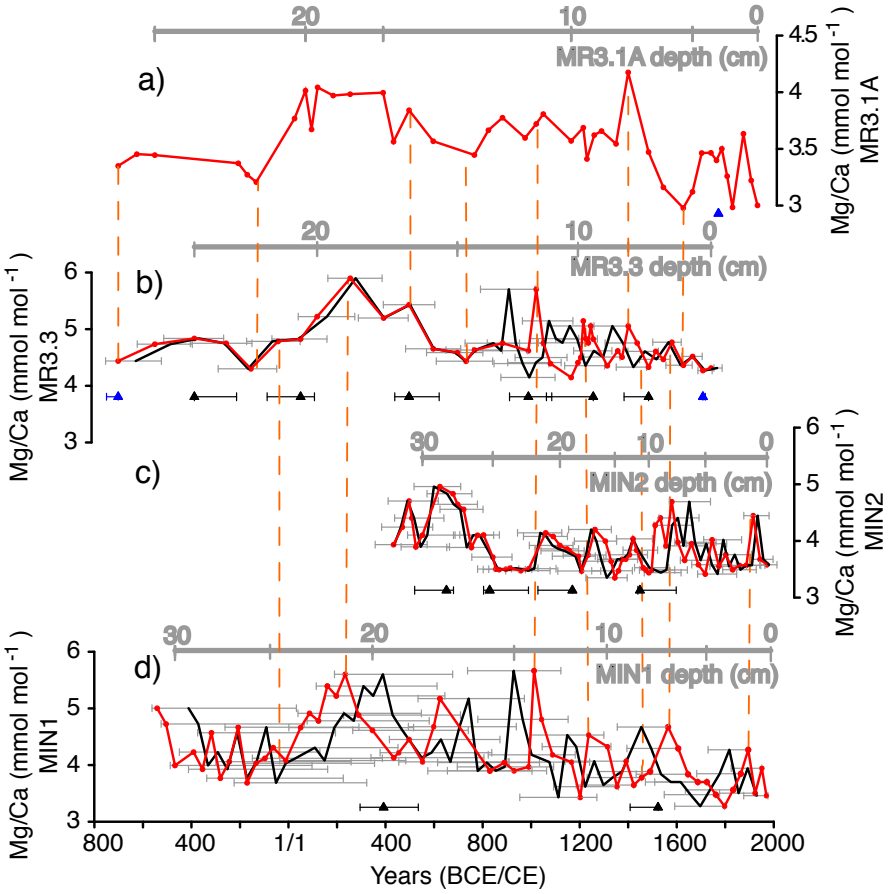

Figure S4. Main procedures of multy-proxy chronostratigraphy performed with Mg/Ca records for cores (a) MR3.1A; (b) MR3.3; (c) MIN2, and (d) MIN1. Final age-depth models are plotted in red. Black plots and grey error bars correspond to Bayesian accumulation age-depth models. Triangles represent to ^{14}C dates (black) and biostratigraphical dates based on planktonic foraminifera (blue), and they are shown below the corresponding core and with their associated 2 σ errors. Depths in relation to the final age model can be observed above its corresponding core. Vertical dashed lines (orange) indicate tie points between the different Mg/Ca records (tie points and attendant uncertainties in Table S4).

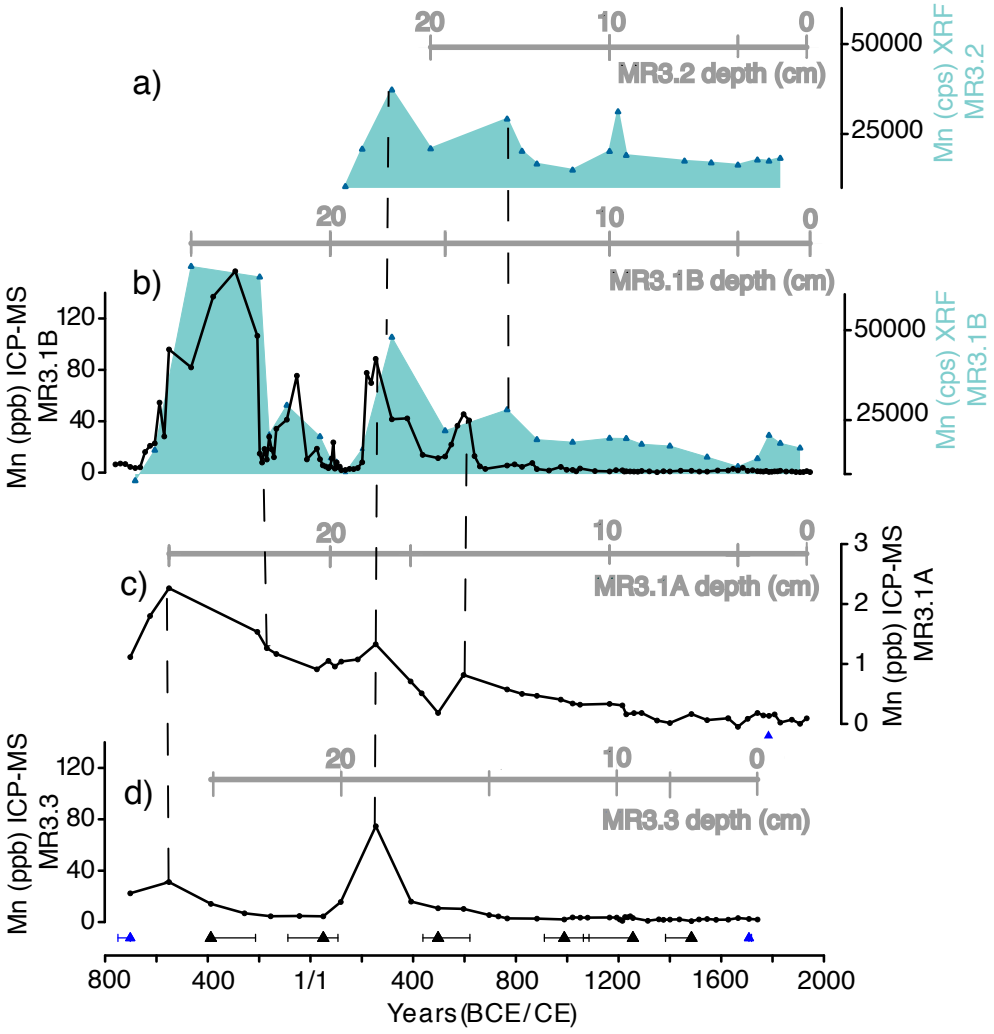

Figure S5. Multy-proxy chronostratigraphy performed with Manganese profiles. Blue filled plots represents Mn profiles obtained by XRF Core-Scanner for cores (a) MR3.2, and (b) MR3.1B, respectively. Black plots show Mn from trace elements analysed by means of ICP-MS for cores (b) MR3.1B, (c) MR3.1A, and (d) MR3.3. Vertical dashed lines indicate tie points of geochemical chronostratigraphy (tie points and attendant uncertainties in Table S1). Triangles represent to ^{14}C dates (black) and biostratigraphical dates based on planktonic foraminifera (blue) and they are shown below the corresponding core and with their associated 2 σ errors.